Real-time in vivo ROS monitoring with luminescent nanoparticles reveals skin inflammation dynamics

M. Abdesselem, N. Pétri, R. Kuhner, F. Mousseau, V. Rouffiac, T. Gacoin, C. Laplace-Builhé, A. Alexandrou, C I Bouzigues

Research Article | Vol. 14, No. 10 / 1 Oct 2023 / Biomedical Optics Express 5392
Biomedical Optics EXPRESS

Real-time *in vivo* ROS monitoring with luminescent nanoparticles reveals skin inflammation dynamics

M. ABDESSELEM,[1,†] N. PÉTRI,[1,†] R. KUHNER,[1] F. MOUSSEAU,[1] V. ROUFFIAC,[2] T. GACOIN,[3] C. LAPLACE-BUILHÉ,[2] A. ALEXANDROU,[1,‡] AND C. I. BOUZIGUES[1,‡]

[1]*Laboratory for Optics and Biosciences, Ecole polytechnique, Institut Polytechnique de Paris, CNRS, INSERM, 91128 Palaiseau cedex, France*
[2]*Photon Imaging and Flow Cytometry, CNRS, INSERM, Gustave Roussy Cancer Campus, 114, rue Edouard Vaillant, 94805 Villejuif Cedex, France*
[3]*Laboratoire de Physique de la Matière Condensée, Ecole polytechnique, Institut Polytechnique de Paris, CNRS, 91128 Palaiseau cedex, France*
[†]These authors contributed equally to this work
[‡]These authors jointly supervised this work

Abstract: Reactive oxygen species (ROS) are key regulators in numerous pathological contexts, including cancer or inflammation. Their role is complex, which justifies the need for methods enabling their quantitative and time-resolved monitoring *in vivo*, in the perspective to profile tissues of individual patients. However, current ROS detection methods do not provide these features. Here, we propose a new method based on the imaging of lanthanide-ion nanoparticles ($GdVO_4$:Eu), whose photoluminescence is modulated by the surrounding ROS concentration. We monitored their luminescence after intradermic injection in a mouse ear submitted to an inflammation-inducing topical stimulus. Based on this approach, we quantified the ROS concentration after inflammation induction and identified a two-step kinetics of ROS production, which may be attributed to the response of resident immune cells and their further recruitment at the inflammation locus.

1. Introduction

Reactive Oxygen Species (ROS) have long been known for their role in fighting and degrading pathogens by the immune system through the phagocytosis process [1–3]. More recently, H_2O_2, in particular, has been shown to be an ubiquitous secondary messenger molecule, involved in a large variety of signaling processes [4,5]. In the latter case, H_2O_2 concentrations may remain low on the 1-10 µM range, and are tightly regulated in space and time as their homeostasis is crucial for the balance between their beneficial and deleterious roles [5–7]. It has thus been hypothesized that the impairment of ROS regulation is involved in numerous pathologies, such as cancers, or as neurodegenerative [8–11] and, more generally, inflammation-related, diseases. Oxidative stress has thus been long identified as an important element in Parkinson's disease [12] and ROS concentration may regulate neurodegeneration and neuronal death [13]. In inflammation, ROS constitute an important component of the inflammation condition along with cytokines, chemokines and enzymes, and is involved in the initiation, progression, and resolution of the inflammatory response [14,15]. Their role is complex in wound healing and immune response regulation [14], notably through immune cell chemotaxis and recruitment [16] or proliferation [17].

Furthermore, ROS play an important, although controversial, role in cancer [18]. The relation between chronic inflammation and cancer has been established, *e.g.* in the case of *Helicobacter pylori* infection leading to gastric ulcer disease, which may then evolve into gastric cancer

#501914 https://doi.org/10.1364/BOE.501914
Journal © 2023 Received 28 Jul 2023; revised 30 Aug 2023; accepted 31 Aug 2023; published 25 Sep 2023

Biomedical Optics EXPRESS

[19,20] and tumors often display high ROS levels. For this reason, several anti-inflammatory drugs are successful anticancer drugs [18]. Nevertheless, the idea that ROS and the related oxidative stress may only be responsible for increased mutation rates and for the transformation of healthy cells into cancerous cells thus initiating tumors and favoring tumor progression [21] has proven to be oversimplified. Indeed, ROS production may cause cancer cell death, where ROS-related oxidative stress was actually found to inhibit metastasis of melanoma cells through blood circulation by efficiently eliminating cancer cells released from solid tumors [22,23]. It has furthermore been reported to up-regulate the activation of tumor suppressors [24]. Therefore, both anti-oxidant and pro-oxidant treatments have been tested to treat various cancer types [25].

This degree of complexity means that ROS production and prevalence, in the broad range of conditions and diseases in which it is involved, needs to be accurately assessed *in vivo* with adequate sensor tools, which should provide a quantitative and time-resolved detection. The *in situ* monitoring of ROS in tissues is thus necessary, (i) to determine accurately their oxidative profiles, (ii) to decipher the mechanisms of their production and patho-physiological effects. The further correlation with clinical observation could then contribute to personalized diagnosis and treatment assessment.

A variety of ROS or specific H_2O_2 detection methods exist and have been implemented in *in vitro* measurements related to cell activity, relying either on electrochemical [26,27], radiological [28], MRI [29] or optical [7,30–35] approaches. However, their applications for ROS detection in living organisms have remained sparse [34,35] and provide only poorly time-resolved and qualitative measurements. Optical approaches rely on the use of chemiluminescent or fluorescent probes. Amongst the latter ones, variants of a genetically encoded sensor, the redox sensitive Hyper [30,36], have been efficiently implemented *in vivo* to image wound healing at the tail of zebrafish embryos [37]. Though efficient to reveal reversible oxidative processes, this approach, besides requiring genetically modified organisms, is suitable for sub-micromolar H_2O_2 concentrations only due to the saturation of the sensor signal, which precludes any quantitative monitoring of ROS production during inflammatory responses *in vivo*.

We have demonstrated that Eu-doped $Y_{0.6}Eu_{0.4}VO_4$ or $Gd_{0.6}Eu_{0.4}VO_4$ nanoparticles were efficient ROS probes *in vitro* [6,7,38], with a concentration-dependent response time between 30 and 300 s in the micromolar range. We moreover demonstrated intracellular quantitative, space and time-resolved H_2O_2 detection with respective space and time resolutions of 40 nm and down to 30 s with the use of a single nanoparticle type [38] and 1 s in a ratiometric approach [39], in the range of 1 to 45 µM H_2O_2. Using this nanosensor, we could demonstrate that the temporal dynamics upon stimulation of vascular smooth muscle cells (VSMC) is different depending on the type of stimulation and that an intracellular H_2O_2 gradient builds up in the case of stimulation by an external ligand gradient [7]. Although these particles do not respond specifically to H_2O_2 alone but more generally to strong oxidants, such as ClO^-, we have shown, for the cell processes discussed above, that they may exclusively detect H_2O_2 in the absence of other stable ROS at high enough concentrations [6,7]. In a more complex environment involving the production of multiple ROS types, these sensors can be used as ROS and not only H_2O_2 sensors.

The absence of signal saturation even for high concentrations of H_2O_2 up to 5 mM [6] implies that these nanoparticles are suitable for quantitative detection in a range tunable by their excition conditions. Moreover, $GdVO_4$:Eu nanoparticles present a low toxicity, either *in vitro* after 48 h internalization in cells, in which they do not induce significant cytotoxicity [39] or after intravenous injection in mice, which do not exhibit any physiological alterations several hours after injection [38].

Altogether, these elements support the use of $GdVO_4$:Eu nanoparticles for monitoring inflammation-related processes *in vivo*, during which high ROS concentrations may be produced.

We here present measurements of ROS concentration *in vivo* in a mouse inflammation model using $Gd_{0.6}Eu_{0.4}VO_4$ nanosensors. We validated the inflammation model with fluorescence

Biomedical Optics EXPRESS

angiography and performed control experiments showing that the luminescence signal from $Gd_{0.6}Eu_{0.4}VO_4$ nanoparticles injected into the ear tissue is detectable and shows an inflammation-induced rise. We could thus demonstrate a two-step *in vivo* response in ROS upon inflammation induction: a fast and a delayed response that we attribute to resident and recruited leucocytes, respectively.

2. Results and discussion

Nanoparticle H_2O_2 response characterization. To detect ROS in living tissues, we first demonstrated the feasibility to image $Gd_{0.6}Eu_{0.4}VO_4$ in thick samples in order to semi-quantitatively monitor their redox state. Direct absorption of Eu^{3+} ions in $Gd_{0.6}Eu_{0.4}VO_4$ nanoparticles takes place at 466 and at 396 nm [38,39] and the subsequent emission is centered at 617 nm (Figure S1). Due to possible photodamages under UV excitation, in *in vivo* experiments, excitation at the higher wavelength of 466 nm is preferable and was thus used (Material and Methods). The penetration in tissues at this wavelength is however limited, and appropriate only for imaging in the vicinity of the dermis, such as tissues in the mouse ear.

We first chemically reduced the nanoparticles using $NaBH_4$ as reported in [38] to avoid the requirement of photoreduction *in vivo* before ROS sensing, whose intensity and duration [6,7] could damage the tissues in *in vivo* experiments. Given that the absorption peak of Eu^{3+} ions is not significantly modified upon chemical reduction [38], we assume that the chemical reduction process introduces quenching sites for the Eu^{3+} emission, such as V^{4+}, leading to a loss of luminescence.

To quantify the photoluminescence (PL) response of the nanoparticles to H_2O_2 in a situation comparable to tissue imaging, we injected the nanoparticle solution in a 10% agarose gel piece, which was then imaged with a macroscope (Material and Methods) under a 466 nm illumination (Fig. 1(A)). In this quite dense material, the mobility of $GdVO_4$:Eu nanoparticles is highly limited (Fig. 1(B)), similarly to what occurs in living tissues (see below). Absence of diffusion is a key factor because, in the presence of facile diffusion, the nanoparticle signal would become too weak to be observable under a macroscope. We then added solutions of different H_2O_2 concentrations to the sample holder containing the gel piece (Fig. 1). While the nanoparticle luminescence remains stable in the absence of oxidant, we observed a concentration-dependent recovery of the luminescence after H_2O_2 addition (Fig. 1(B), C) between 0 and 100 µM, over which a quasi-full re-oxidation is reached under our excitation conditions. This demonstrates the feasibility of detecting ROS through $GdVO_4$:Eu nanoparticle imaging in a gel in this concentration range. To avoid artifacts due to the variability of the H_2O_2 diffusion time within the gel, we considered the response after a long time (30 min) of incubation. This steady-state response of agarose-dispersed nanoparticles is linear in the 0-100 µM range (Fig. 1(C)): this result can thus be used as a calibration table. The kinetics of the recovery is indeed not extracted from this observation, since it is both limited by the nanosensor response [6,39] and the H_2O_2 diffusion from the solution into the agarose gel (Figure S2).

***Acute skin inflammation in mice*.** Inflammation models in mice are often complex and have given rise to controversial conclusions concerning their relevance for mimicking human diseases [40,41]. We here used a model of acute skin irritation established since the 1990s as the so-called mouse ear swelling test [42,43] with a recent adaptation from Kalchenko et al. [44] for topical application of a known strong primary irritant and potential allergen: methylsalicylate (MS). This model is known for inducing an acute vascular response immediately after topical application, which results in longer-term macroscopic changes such as ear thickness increase and redness.

We characterized the vascular skin inflammatory response to a topical application of MS by systematic injection of a fluorescent reporter (Dextran-TRITC) in the blood circulation and imaging of the ear vasculature using fluorescence and transmission imaging [45] (Fig. 2). Prior to MS application, the ear vasculature is typical of normal healthy animals with fluorescent signal

Biomedical Optics EXPRESS

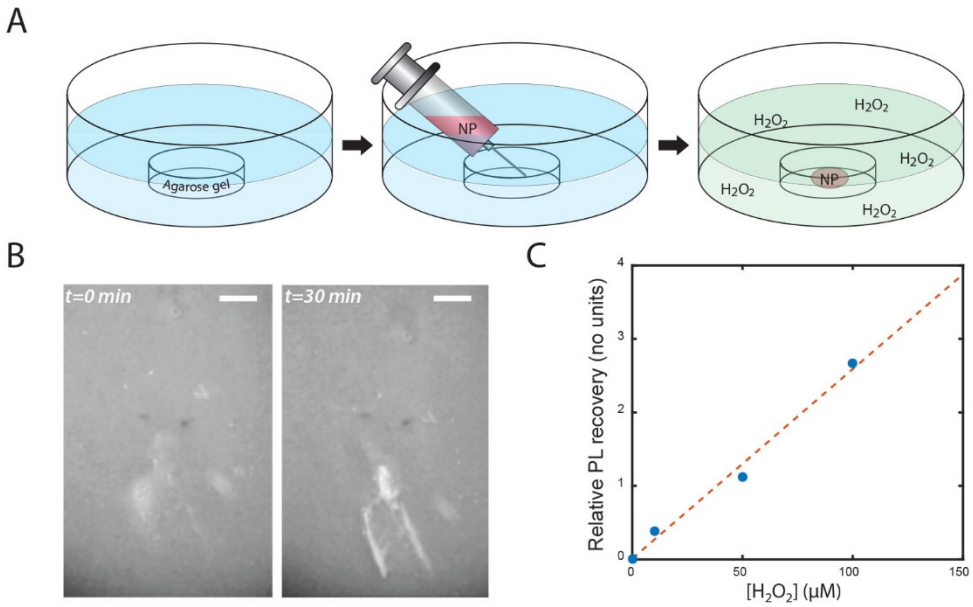

Fig. 1. (A) Preparation of calibration samples. (B) Typical image of an agarose gel after nanoparticle injection. The inhomogeneity in the nanoparticle dispersion is due to their poor diffusion in dense agarose gel. The location of the gel containing the nanoparticles is slightly shifted at the moment of the H_2O_2 addition. Scale bar: 500 μm. (C) Relative photoluminescence PL recovery after 30 min incubation with different H_2O_2 concentrations (PL(t = 30 min)/PL(t = 0 min)-1).

only originating from well-defined vessels (Fig. 2(A)). In contrast, 5 minutes after application of the irritant, the ear vasculature is dramatically modified with larger and ill-defined vessels (Fig. 2(B)). The diffuse signal around blood vessels depicts leakage of the fluorescent probe into the surrounding tissue.

We monitor the blood supply in the observed skin region through angiography by imaging TRITC fluorescence injected intravenously and recording the vascularization evolution after irritant application. We first observed a MS induced blood flow increase, revealed by the fluorescence intensity increase of single vessels due to their broadening (Fig. 2(C)). In addition, vessel permeabilization leads to TRITC-dextran extravasation, which also contributes to the whole-field fluorescence increase. A 3-fold increase in fluorescence signal is observed over ten minutes starting approximately 100 s after irritant application. (Figure 2(C), blue line). Moreover, 10 min after MS application, the acquired transmission image is darker than before application (Figs. 2(E), F). Quantification of the transmission signal over the whole image shows a decrease of 10% due to hemoglobin absorption after blood suffusion (Fig. 2(D)). Altogether, these results confirm the efficiency of the ear inflammation model proposed here, which induces typical inflammation-associated vasomotor effects, like blood flow increase. We furthermore can estimate the kinetics of this process in this system, with a typical increase of the vascularization ~100-200 s after MS stimulation.

In vivo ROS dynamics. To measure ROS dynamics upon mouse ear inflammation, we placed anesthesized mice, whose ears were shaved to reduce light scattering and emission from hair follicles (Fig. 3(A)), under a macroscope, which was equipped with a laser diode emitting at 466 nm (see Material and Methods) for excitation of the nanosensor luminescence and with a filter for detecting the nanoparticle emission centered at 617 nm (Fig. 3(B)). We injected a small

Biomedical Optics EXPRESS

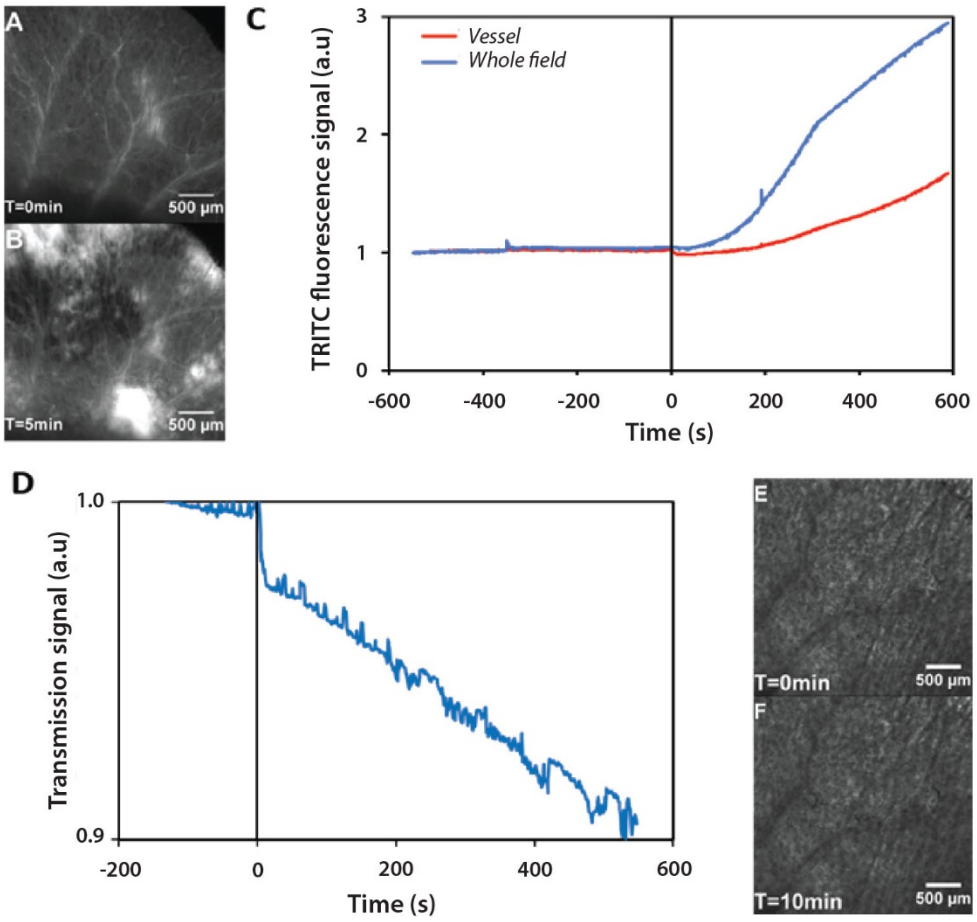

Fig. 2. Ear swelling irritation model. Observation of mouse ear vasculature upon antero-orbital (systemic) injection of approximately 50 µL of dextran-TRITC (A) before methylsalicylate application and (B) 5 minutes after the irritant application. (C) Time evolution of the total fluorescence signal in the image (blue line) and signal for a single vessel (red line) starting 10 minutes before methylsalicylate application and until 10 minutes after. (D) Time evolution of the total transmission signal of the mouse ear starting 2 minutes before methylsalicylate application and until 10 minutes after obtained from images like those shown in (E) just before methylsalicylate application and (F) 10 minutes after the irritant application. The black line shows the time point of methylsalicylate application.

Biomedical Optics EXPRESS

volume (approx. 10 µL) of chemically reduced $Gd_{0.6}Eu_{0.4}VO_4$ ([V] = 10 mM) nanoparticles in the mouse ear dermis (Fig. 3(A), C). A white-light image was first acquired to ensure that the ear was not pierced during the injection and that the suspension was indeed injected in the ear tissue. We then detected the nanoparticle luminescence upon 466-nm excitation either still localized (Fig. 3(D)) at the injection locus or scattered in the surrounding tissue (Fig. 3(E)), depending on the variability of the tissue properties and of the injection procedure. The total luminescence may result from nanoparticle emission and from endogenous fluorescence, notably from remaining hair follicles. However, the absence of fluorescence under different excitation wavelengths (excitation at 377 nm or 550 nm, with the same power as at 466 nm, Figs. 3(F)-(H)) confirms that the detected signal at 617 nm (Fig. 3(F)) is due to the presence of nanoparticles.

The nanoparticles are large enough (30 nm) so that they do not diffuse inside the mouse ear tissue after injection. Indeed, no significant deformation of the nanoparticle luminescence spatial profile is observed as a function of time (Fig. 4(A)-(B), Visualization 1). This is similar to what was observed in the cell cytosol where individual $Gd_{0.6}Eu_{0.4}VO_4$ nanoparticles remained practically immobile [39]. In the mouse ear, the extracellular matrix environment where the particles are injected is probably too dense to allow diffusion of the 30 nm nanoparticles, which thus provides spatial resolution, in contrast with freely diffusing small organic ROS sensors. Furthermore, no photobleaching of nanoparticles can be observed (inset Fig. 4(C)), which enables long-term imaging and quantitative analysis of the luminescence signal to estimate the ROS concentration evolution.

We then measured the luminescence signal of the injected $Gd_{0.6}Eu_{0.4}VO_4$ nanoparticles during 2 minutes before irritant application and we observed a stable photoluminescence signal (inset Fig. 4(C)), as in agarose gels in the absence of H_2O_2. No significant oxidant concentrations were thus detectable by our probe and consequently no measurable oxidant stress was induced by the nanoparticle injection. Immediately after irritant application (at $t = 0$), we observed the $Gd_{0.6}Eu_{0.4}VO_4$ luminescence signal recovery, which indicates their oxidation after MS-induced inflammation. No significant changes in the response were observed when changing either the injected nanoparticle concentration or their excitation intensity (Fig. S4), which further confirm the absence of nanoparticle-induced effects on the measured response.

The luminescence recovery was measured in MS-treated mice (Fig. 4(C)), and all of those where nanoparticle could be detected exhibited a significant response (average relative PL recovery amplitude A =0.8 +/- 0.1 (s.e.m), n = 6) on the contrary of unstimulated mice (Fig. 4(C)). We then performed a quantitative evaluation of the signal, based on the relative enhancement of the oxidative response revealed by the luminescence increase, which reveals the kinetics of the ROS response. The average signal before MS application is normalized to 1 and the luminescence recovery is shown as the difference with respect to the normalized signal before MS application. Luminescence recovery occurs in two steps (Fig. 4(C), D): (i) a weak (~30% of photoluminescence recovery) a few seconds after MS application before vasculature alteration which takes 100-200 s (Fig. 2(C)), and/or (ii) a strong response occurring a few minutes after MS application, after the beginning of the vascularization changes. A heuristic Hill type time response function (Fig. 4(C), dashed lines), resulting from an extended auto-catalytic Prout-Tompkins model [46,47], quantitatively accounts for this behavior; displaying a fast component and a slow one with respective half-height times T_{fast}=21 ± 9 s and T_{slow}=300 ± 60 s (Fig. 4(E)). Since the fast recovery time T_{fast} is comparable to the expected $GdVO_4$:Eu response [6,38,39], it most probably does not directly describe the ROS production kinetics, whose typical time T^*_{fast} may be shorter than T_{fast} (T_{fast}<T^*_{fast}).

All the recorded responses exhibit either one of these components or, in most cases (n = 4 over 6 mice), both a weaker fast response and a strong, delayed response are observed (Fig. 4), with respective average relative recovery amplitudes A_{fast}=0.12 ± 0.05 and A_{slow}=0.7 ± 0.1 (Fig. 4(D)). In contrast, acetone-treated mice did not exhibit any significant responses (Supplement 1, Fig.

Biomedical Optics EXPRESS

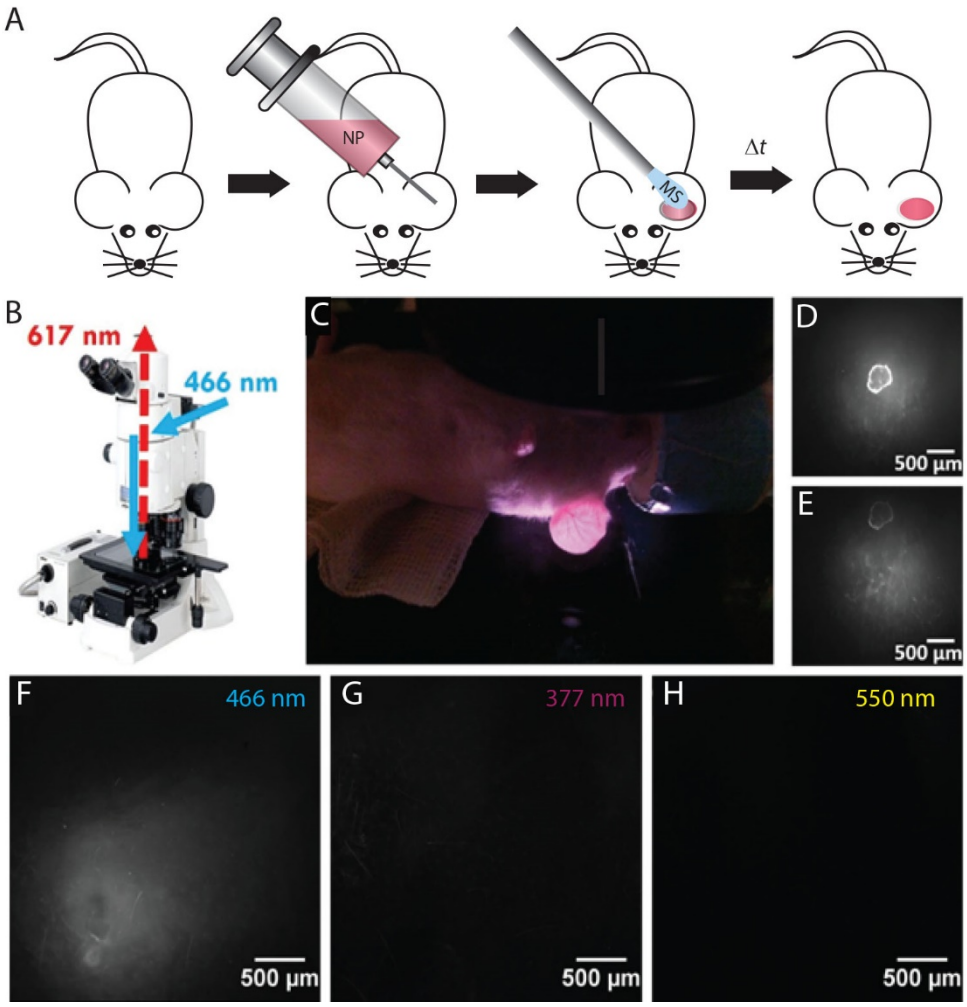

Fig. 3. Experimental setup and control images. (A) Principle of MS-induced ROS production monitoring: (i) direct injection of nanoparticles in the mouse ear, (ii) topic application of MS, (iii) luminescence monitoring. (B) Macroscope configuration for ROS detection using $Gd_{0.6}Eu_{0.4}VO_4$ nanoparticles. (C) Image of a mouse ear under the macroscope. Observation of luminescence at 617 nm upon intradermic injection of approximately 10 µL of $Gd_{0.6}Eu_{0.4}VO_4$ nanoparticles (D) centered on the injection site, (E) next to injection site (bright spots are hair follicles). Observation of particle luminescence at the injection site with a collection filter centered at 617 nm under excitations at (F) 466 nm, (F) 377 nm and (H) 550 nm. The same grey scale was used for all three images F-H. (Note that the dark spot observed at the bottom left of the nanoparticle emission is probably due to local skin damage caused by the injection needle).

Biomedical Optics EXPRESS

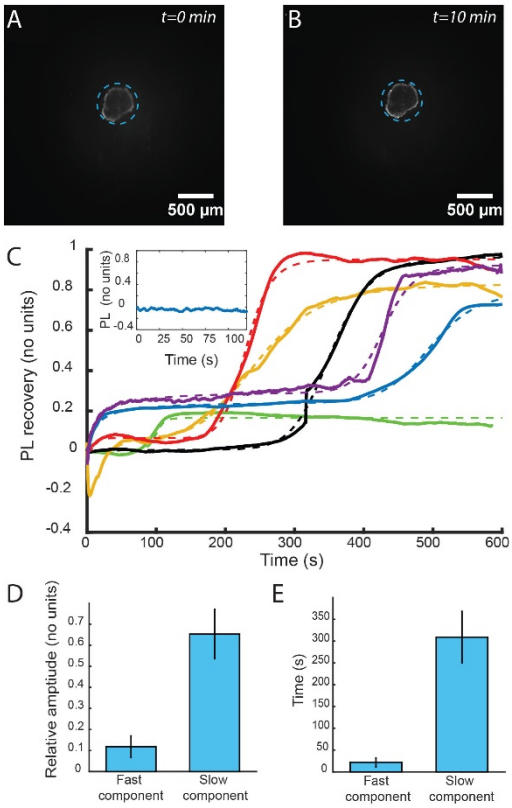

Fig. 4. ROS concentration dynamics during skin inflammation. Raw image of $Gd_{0.6}Eu_{0.4}VO_4$ nanoparticles injected into a mouse ear, under 466 nm laser illumination, (A) before methylsalicylate application and (B) 10 min after application. The analyzed region is shown by the blue dotted circle. The obtained recovery is plotted in black on (C). (C) Luminescence recovery signals (plain lines) of $Gd_{0.6}Eu_{0.4}VO_4$ particles injected in the mouse ear shown for 6 stimulated mice. Red, blue, purple and yellow curves display a two-step behavior. The recovery signal is obtained by normalizing to 1 the averaged signal just before t = 0 corresponding to the time point of methylsalicylate application and by subtracting from the signal the t = 0 value. The luminescence recovery signals are fitted with a heuristic two-component curves: $A_{fast}\frac{t^{n1}}{t^{n1}+T_{fast}{}^{n1}} + A_{slow}\frac{t^{n2}}{t^{n2}+T_{slow}{}^{n2}}$ (dashed lines, where A, T, n are respectively the amplitudes, the typical times and the Hill coefficients of the responses). Note that the negative signal near t = 0 for the orange curve is an artifact due to the MS application. Insert: example of a photoluminescence signal after nanoparticle injection in the absence of MS application. Average amplitudes (A_{fast} and A_{slow}) (D) and half-height recovery times (E) (T_{fast} for responses in which a significant slow component is detected (n = 4) and T_{slow}) resulting from the fits in (C) (error bars represent the standard error on the mean).

Biomedical Optics EXPRESS

S3), which excludes any artefactual solvent effect, and neither higher nanoparticle concentration or illumination intensity appears to significantly impact this response (Supplement 1), which confirms that the recorded signal is only due to the MS stimulation. Based on the *in vitro* calibration (Fig. 1), we estimate the typical effective ROS concentrations reached after each step: $C_{fast} \sim 5$ µM and $C_{slow} \sim 30$ µM.

However, the possible presence of multiple oxidant species (H_2O_2 but also short-lived and highly reactive ClO^-, $O_2^{\cdot -}$, $HO^{\cdot -}$, . . .) during the inflammation process, and the lack of specificity of $GdVO_4$:Eu nanoparticles for strong oxidant detection, may complexify the interpretation of this concentration estimation. Indeed, while hydroxyl radicals and superoxide ions are short-lived in biological environements [48] and are unlikely to be detected by $GdVO_4$:Eu nanoparticles, which have a response time in the minute range, the role of ClO^- has notably been reported in inflammation processes [49,50] and tts contribution to the particle re-oxidation and thus luminescence recovery cannot be excluded. Our concentration estimation *in vivo* are a measurement of the effective oxidative response due to all produced ROS, expressed in H_2O_2 concentration units – *i.e.* the H_2O_2 concentration able to elicit a similar reoxidation-, in contrast to our previous work on the ROS response in intracellular signaling processes, where pharmacological treatments could ensure that H_2O_2 was the sole oxidant present [6].

The comparison of the kinetics of the ROS response (Fig. 4(C)) with the vasculature modifications in this inflammation model (Fig. 2(C)) confirms the entanglement of ROS production and vascular inflammation response widely reported in the literature [14,51–54]. The fast response may occur faster than the sensor temporal resolution [38], before any measurable vascular effect, which indicates that ROS are probably produced by patrolling immune cells during the initial stage of inflammation [14,52,54]. The inflammatory response involves the further recruitment of immune cells (neutrophils, macrophages, and lymphocytes) in tissues through their adhesion, migration [16,52,55], or proliferation [17] and vascular modifications including vasodilatation, blood flow increase [56,57] and angiogenesis [58]. Based on the observation that the strong and slow ROS response occurs shortly (T_{slow}=300 ± 60 s, Fig. 4(E)) after the vascularization effects (Fig. 2(C)), we can hypothesize that this response is the contribution to ROS production of newly recruited immune cells through the increased blood circulation (Fig. 5). Indeed, previous observations in acute inflammation models showed similar fast kinetics with vascular effects [44] or monocyte and neutrophil recruitment [59,60] being detected less than 30 min after the stimulation. Interestingly, the amplitudes of the fast and slow components are different from one animal to another (Fig. 4(C)), which may be related to the difference in the nanoparticle localization within the tissue or to the subject-dependent variability in the immune response [61].

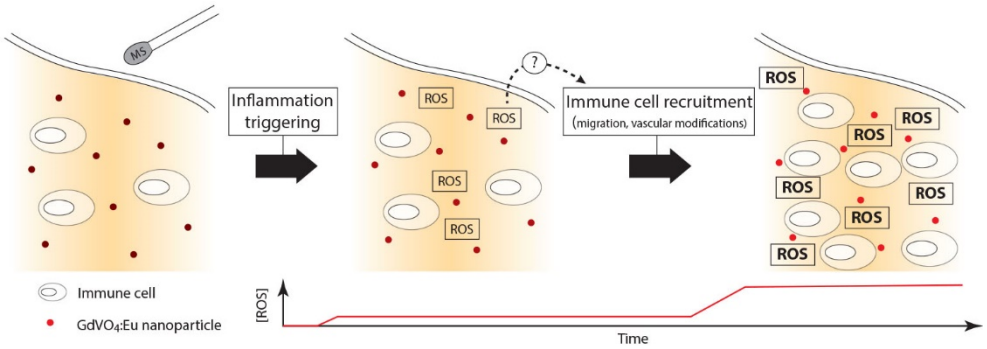

Fig. 5. Model of ROS production kinetics in ear tissues after inflammation triggering by MS.

Biomedical Optics EXPRESS

These results demonstrate the feasibility of using photoluminescence measurements of lanthanide-based particles to profile tissues ROS production *in situ* and form the basis for the development of novel personalized diagnostics methods. Future work should narrow down the specific contribution of H_2O_2 and other oxidants by using pharmacological treatments, *e. g.* with catalase as shown in the case of our previous intracellular experiments [6,7].

3. Conclusions

Altogether, these results demonstrate the feasibility of semi-quantitative measurements, *i.e.* through the estimation of an equivalent H_2O_2 concentration, of the ROS production dynamics during an inflammatory response through luminescent nanoparticle imaging. The combination of these measurements with functional imaging (angiography) provides an accurate characterization of the tissue response, in the context of acute inflammation, both at the functional and molecular scale. This paves the way for the further development, possibly in association with endoscopy to circumvent the low penetration of blue excitation, of quantitative tissue profiling methods, which could be used for *in situ* inflammation or cancer monitoring in the context of personalized diagnosis.

4. Methods

Animals and reagents. OF1 7 weeks old mice were anesthetized with isoflurane inhalation. The isoflurane flow rate was adjusted between 0.3 L/min and 0.8 L/min in order to maintain stable respiratory rates and the light anesthesia required for imaging. Irritation of the external ear was induced by topically applying a tissue soaked with methylsalycilate (MS) solution (Sigma Aldrich, pure MS 99.9%) diluted ten times in pure acetone (Sigma Aldrich). We performed vasculature imaging after antero-orbital injection of tetramethylrhodamine isothiocyanate (TRITC)–dextran solution (Sigma Aldrich, average molecular weight 4,400 g.mol^{-1}) at a concentration of 50 µg/mL in PBS. All injections were performed with 30 G syringe needles.

Animals received human care and the study protocols complied with GRCC guidelines for the care and use of laboratory animals.

Nanoparticle preparation. We prepared nanoparticles of $Gd_{0.6}Eu_{0.4}VO_4$ following the synthesis route reported in Abdesselem et al. [38] (Supplement 1). Briefly, the synthesis consists in mixing a rare-earth nitrate solution (60% Gd, 40% Eu) with sodium orthovanadate solution at room temperature. The two compounds co-precipitate and form polycrystalline $Gd_{0.6}Eu_{0.4}VO_4$ particles with a typical size of 30 nm [38].

These Eu-based nanoparticles are luminescent, photostable and sensitive to their ROS environment [38]. We reduced $Gd_{0.6}Eu_{0.4}VO_4$ particles ([V] = 10 mM) with a 1 M solution of $NaBH_4$ during 5 minutes. Then the excess reducer was discarded by 5 successive centrifugations at 5000 g during 5 minutes and washings with pure water. No spontaneous luminescence recovery was observed during several hours [39].

The surface charge of non-coated $Gd_{0.6}Eu_{0.4}VO_4$ particles is low (ζ-potential = 8.6 mV). The suspension was hence supplemented with polyacrylic acid (PAA; Sigma-Aldrich, 25 µL/mL yielding a PAA concentration of 3.6 mg/ml) and sonicated during several minutes (3×1 minute). The hydrodynamic diameter of this nanoparticle preparation was measured with dynamic light scattering (DLS) and yielded a peak of the number distribution at 50 nm with a polydispersity index of 0.2. Note that DLS measurements emphasize the contribution of large particles to the size distribution leading to a systematic size overestimation of colloids that are not strictly monodisperse.

***In vitro* calibration.** Agarose gel (10% agar in PBS 1X) pieces (~5×5x5 mm) were cut and placed on a coverslip inside a sample holder, which was then covered with PBS buffer. Reduced nanoparticle solution (10 µl, [V] = 4.5 mM) was then injected through a syringe within the gel. The buffer was then replaced by a solution of PBS prepared extemporaneously containing a known

Biomedical Optics EXPRESS

H_2O_2 concentration (0, 10, 50, 100 µM) and imaging was performed through a macroscope (Zeiss AxioZoom.V16 macroscope, Hamamatsu ORCA-Flash4 camera) under illumination at 466 nm through a diode laser (Modulight) during 30 min in the very same experimental conditions as for the animal experiments (see below), *i.e.* 5 mW laser power at the sample and beam size of 5 mm.

***In vivo* imaging.** Imaging was performed with a Nikon Axiozoom AZ100 zoom-macroscope in two different modes: (1) white light transmission to monitor intradermic injections and (2) fluorescence/luminescence emission. For the second mode, the setup was supplemented with a 466-nm diode laser (Modulight) for luminescence excitation of Eu-based nanoparticles and TRITC-dextran. Excitation was performed through the objective (Magnification x2, numerical aperture NA = 0.2) at a zoom of 1.3, yielding a beam size of ~5 mm. The laser power was 5 mW, thus yielding a typical excitation intensity of 6 mW.cm^{-2}. Emitted photons from Eu^{3+} ions and TRITC were detected through band pass filters, 617 ± 8 nm (Semrock) and 625 ± 40 nm (Chroma), respectively, with an EM-CCD camera (Luca, Andor Technology). Excitation at 377 and 550 nm (Figs. 2(F) and (G)) was obtained with a metal halide lamp and appropriate excitation filters. For the acquisition of the nanoparticle emission signal, the typical exposure time was 900 ms and the acquisition rate was 1 frame per second.

10 µL of the reduced nanoparticle solution stabilized with PAA were injected in the mouse ear with a 30 G syringe needle while imaging the injected area with the macroscope. A near 90° injection angle was used to obtain nanoparticle injection in the area between the two ear dermis layers. Particular care was taken to avoid release of nanoparticle solution on the top mouse ear dermis or below the bottom ear dermis. The external ear of anesthetized animals was then continuously imaged for 2 minutes before application of the irritant and typically for 10 minutes after MS application.

Funding. Agence Nationale de la Recherche (ANR-10-INBS-04).

Acknowledgements. This work was evaluated by an ethics committee on animal experimentation and authorized under project number AP AFIS#6630-20 16090608316724 v3.

Author Contributions Statement. M.A, N.P, R.K, F.M. and V.R. performed experiments. T.G., C.L-B, A.A. and C.B designed experiments. M.A., N.P, R.K. and C.B. analyzed the data. M.A, F.M., R.K. A.A. and C.B. wrote the paper.

Disclosures. The authors declare no conflicts of interest.

Data availability. Data underlying the results presented in this paper are not publicly available at this time but may be obtained from the authors upon reasonable request.

Supplemental document. See Supplement 1 for supporting content.

References

1. C. W. Baldridge and R. W. Gerard, "The Extra Respiration of Phagocytosis," American Journal of Physiology-Legacy Content **103**(1), 235–236 (1932).
2. B. M. Babior, J. T. Curnutte, and B. J. McMurrich, "The Particulate Superoxide-Forming System from Human Neutrophils. Properties of the System and Further Evidence Supporting Its Participation in the Respiratory Burst," J. Clin. Invest. **58**(4), 989–996 (1976).
3. S. Dupré-Crochet, M. Erard, and O. Nüße, "ROS Production in Phagocytes: Why, When, and Where?" J. Leukocyte Biol. **94**(4), 657–670 (2013).
4. S. G. Rhee, "CELL SIGNALING: H2O2, a Necessary Evil for Cell Signaling," Science **312**(5782), 1882–1883 (2006).
5. B. D'Autréaux and M. B. Toledano, "ROS as Signalling Molecules: Mechanisms That Generate Specificity in ROS Homeostasis," Nat. Rev. Mol. Cell Biol. **8**(10), 813–824 (2007).
6. D. Casanova, C. Bouzigues, T.-L. Nguyên, R. O. Ramodiharilafy, L. Bouzhir-Sima, T. Gacoin, J.-P. Boilot, P.-L. Tharaux, and A. Alexandrou, "Single Europium-Doped Nanoparticles Measure Temporal Pattern of Reactive Oxygen Species Production inside Cells," Nat. Nanotechnol. **4**(9), 581–585 (2009).
7. C. I. Bouzigues, T.-L. Nguyên, R. Ramodiharilafy, A. Claeson, P.-L. Tharaux, and A. Alexandrou, "Regulation of the ROS Response Dynamics and Organization to PDGF Motile Stimuli Revealed by Single Nanoparticle Imaging," Chem. Biol. (Oxford, U. K.) **21**(5), 647–656 (2014).
8. N Kolodkin, A. Sharma, R. P. Colangelo, A. M. Ignatenko, A. Martorana, F. Jennen, D. Briedé, J. J. Brady, N. Barberis, M. Mondeel, T. D. G. A. Papa, M. Kumar, V. Peters, B. Skupin, A. Alberghina, L. Balling, R. Westerhoff, and Hans V. Westerhoff, "ROS Networks: Designs, Aging, Parkinson's Disease and Precision Therapies.," npj Syst. Biol. Appl. **6**(1), 34 (2020).

Biomedical Optics EXPRESS

9. M. Hemmati-Dinarvand, S. Saedi, M. Valilo, A. Kalantary-Charvadeh, M. Alizadeh Sani, R. Kargar, H. Safari, and N. Samadi, "Oxidative Stress and Parkinson's Disease: Conflict of Oxidant-Antioxidant Systems," Neurosci. Lett. **709**, 134296 (2019).
10. J. N. Peoples, A. Saraf, N. Ghazal, T. T. Pham, and J. Q. Kwong, "Mitochondrial Dysfunction and Oxidative Stress in Heart Disease," Exp Mol Med **51**(12), 1–13 (2019).
11. E. Dubois-Deruy, V. Peugnet, A. Turkieh, and F. Pinet, "Oxidative Stress in Cardiovascular Diseases.," Antioxidants **9**(9), 864 (2020).
12. V. Dias, E. Junn, and M. M. Mouradian, "The Role of Oxidative Stress in Parkinson's Disease," J. Parkinson's Dis. **3**(4), 461–491 (2013).
13. P. R. Angelova and A. Y. Abramov, "Role of Mitochondrial ROS in the Brain: From Physiology to Neurodegeneration," FEBS Lett. **592**(5), 692–702 (2018).
14. M. Mittal, M. R. Siddiqui, K. Tran, S. P. Reddy, and A. B. Malik, "Reactive Oxygen Species in Inflammation and Tissue Injury," Antioxid. Redox Signaling **20**(7), 1126–1167 (2014).
15. S. J. Forrester, D. S. Kikuchi, M. S. Hernandes, Q. Xu, and K. K. Griendling, "Reactive Oxygen Species in Metabolic and Inflammatory Signaling," Circ. Res. **122**(6), 877–902 (2018).
16. C. Shi and E. G. Pamer, "Monocyte Recruitment during Infection and Inflammation," Nat. Rev. Immunol. **11**(11), 762–774 (2011).
17. S. J. Jenkins, D. Ruckerl, P. C. Cook, L. H. Jones, F. D. Finkelman, N. Van Rooijen, A. S. MacDonald, and J. E. Allen, "Local Macrophage Proliferation, Rather than Recruitment from the Blood, Is a Signature of T H2 Inflammation.," Science **332**(6035), 1284–1288 (2011).
18. S. M. Crusz and F. R. Balkwill, "Inflammation and Cancer: Advances and New Agents.," Nat. Rev. Clin. Oncol. **12**(10), 584–596 (2015).
19. L. E. Wroblewski, R. M. Peek, and K. T. Wilson, "Helicobacter Pylori and Gastric Cancer: Factors That Modulate Disease Risk," Clin Microbiol Rev **23**(4), 713–739 (2010).
20. B. J. Marshall and H. M Windsor, "The Relation of Helicobacter Pylori to Gastric Adenocarcinoma and Lymphoma: Pathophysiology, Epidemiology, Screening, Clinical Presentation, Treatment, and Prevention," Med. Clin. North Am. **89**(2), 313–344 (2005).
21. M. Valko, M. Izakovic, M. Mazur, C. J. Rhodes, and J. Telser, "Role of Oxygen Radicals in DNA Damage and Cancer Incidence," Mol. Cell. Biochem. **266**(1/2), 37–56 (2004).
22. E. Piskounova, M. Agathocleous, M. M. Murphy, Z. Hu, S. E. Huddlestun, Z. Zhao, A. M. Leitch, T. M. Johnson, R. J. DeBerardinis, and S. J. Morrison, "Oxidative Stress Inhibits Distant Metastasis by Human Melanoma Cells," Nature **527**(7577), 186–191 (2015).
23. I. S. Harris and J. S Brugge. The Enemy of My Enemy Is My Friend. 2.
24. B. Liu, Y. Chen, and D. K. St. Clair, "ROS and P53: Versatile Partnership," Free Radical Biol. Med. **44**(8), 1529–1535 (2008).
25. J. Wang and J. Yi, "Cancer Cell Killing via ROS: To Increase or Decrease, That Is the Question," Cancer Biol. Ther. **7**(12), 1875–1884 (2008).
26. X.-W. Zhang, Q.-F. Qiu, H. Jiang, F.-L. Zhang, Y.-L. Liu, C. Amatore, and W.-H. Huang, "Real-Time Intracellular Measurements of ROS and RNS in Living Cells with Single Core-Shell Nanowire Electrodes," Angew Chem Int Ed Engl **56**(42), 12997–13000 (2017).
27. S. Zhao, G. Zang, Y. Zhang, H. Liu, N. Wang, S. Cai, C. Durkan, G. Xie, and G. Wang, "Recent Advances of Electrochemical Sensors for Detecting and Monitoring ROS/RNS," Biosens. Bioelectron. **179**, 113052 (2021).
28. K. Abe, N. Takai, K. Fukumoto, N. Imamoto, M. Tonomura, M. Ito, N. Kanegawa, K. Sakai, K. Morimoto, K. Todoroki, and O. Inoue, "In Vivo Imaging of Reactive Oxygen Species in Mouse Brain by Using [3 H]Hydromethidine as a Potential Radical Trapping Radiotracer," J. Cereb. Blood Flow Metab. **34**(12), 1907–1913 (2014).
29. R.-W. Tain, A. M. Scotti, W. Li, X. J. Zhou, and K. Cai, "Imaging Short-Lived Reactive Oxygen Species (ROS) with Endogenous Contrast MRI," J. Magn. Reson. Imaging **47**(1), 222–229 (2018).
30. V. V. Belousov, A. F. Fradkov, K. A. Lukyanov, D. B. Staroverov, K. S. Shakhbazov, A. V. Terskikh, and S. Lukyanov, "Genetically Encoded Fluorescent Indicator for Intracellular Hydrogen Peroxide," Nat. Methods **3**(4), 281–286 (2006).
31. E. W. Miller, O. Tulyathan, E. Y. Isacoff, and C. J. Chang, "Molecular Imaging of Hydrogen Peroxide Produced for Cell Signaling," Nat. Chem. Biol. **3**(5), 263–267 (2007).
32. M. Erard, S. Dupré-Crochet, and O Nüße, "Biosensors for Spatiotemporal Detection of Reactive Oxygen Species in Cells and Tissues," American Journal of Physiology-Regulatory Integrative and Comparative Physiology **314**(5), R667–R683 (2018).
33. H. Jin, D. A. Heller, M. Kalbacova, J.-H. Kim, J. Zhang, A. A. Boghossian, N. Maheshri, and M. S. Strano, "Detection of Single-Molecule H2O2 Signalling from Epidermal Growth Factor Receptor Using Fluorescent Single-Walled Carbon Nanotubes," Nat. Nanotechnol. **5**(4), 302–309 (2010).
34. A. Habibalahi, M. D. Moghari, J. M. Campbell, A. G. Anwer, S. B. Mahbub, M. Gosnell, S. Saad, C. Pollock, and E. M. Goldys, "Non-Invasive Real-Time Imaging of Reactive Oxygen Species (ROS) Using Auto-Fluorescence Multispectral Imaging Technique: A Novel Tool for Redox Biology," Redox Biol. **34**, 101561 (2020).
35. L. L. Bronsart, C. Stokes, and C. H. Contag, "Chemiluminescence Imaging of Superoxide Anion Detects Beta-Cell Function and Mass," PLoS One **11**(1), e0146601 (2016).

Biomedical Optics EXPRESS

36. V. V. Pak, D. Ezeriņa, and O. G. Lyublinskaya, *et al.*, "Ultrasensitive Genetically Encoded Indicator for Hydrogen Peroxide Identifies Roles for the Oxidant in Cell Migration and Mitochondrial Function," Cell Metab. **31**(3), 642–653.e6 (2020).
37. D. S. Bilan, L. Pase, L. Joosen, A. Y. Gorokhovatsky, Y. G. Ermakova, T. W. J. Gadella, C. Grabher, C. Schultz, S. Lukyanov, and V. V. Belousov, "HyPer-3: A Genetically Encoded H $_2$ O $_2$ Probe with Improved Performance for Ratiometric and Fluorescence Lifetime Imaging," ACS Chem. Biol. **8**(3), 535–542 (2013).
38. M. Abdesselem, M. Schoeffel, I. Maurin, R. Ramodiharilafy, G. Autret, O. Clément, P. Tharaux, J. Boilot, T. Gacoin, C. Bouzigues, and A. Alexandrou, "Multifunctional Rare-Earth Vanadate Nanoparticles: Luminescent Labels, Oxidant Sensors, and MRI Contrast Agents," ACS nano **8**(11), 11126–11137 (2014).
39. M. Abdesselem, R. Ramodiharilafy, L. Devys, T. Gacoin, A. Alexandrou, and C. I. Bouzigues, "Fast Quantitative ROS Detection Based on Dual-Color Single Rare-Earth Nanoparticle Imaging Reveals Signaling Pathway Kinetics in Living Cells," Nanoscale **9**(2), 656–665 (2017).
40. A. Cauwels, B. Vandendriessche, and P. Brouckaert, "Of Mice, Men, and Inflammation," Proc. Natl. Acad. Sci. U.S.A. **110**(34), E3150 (2013).
41. K. Takao and T. Miyakawa, "Genomic Responses in Mouse Models Greatly Mimic Human Inflammatory Diseases," Proc. Natl. Acad. Sci. U.S.A. **112**(4), 1167–1172 (2015).
42. P. S. Thorne, C. Hawk, S. D. Kaliszewski, and P. D. Guiney, "The Noninvasive Mouse Ear Swelling Assay I. Refinements for Detecting Weak Contact Sensitizers," Fundam. Appl. Toxicol. **17**(4), 790–806 (1991).
43. J.-L. Garrigue, J.-F. Nicolas, R. Fraginals, C. Benezra, H. Bour, and D. Schmitt, "Optimization of the Mouse Ear Swelling Test for in Vivo and in Vitro Studies of Weak Contact Sensitizers *," Contact Dermatitis **30**(4), 231–237 (1994).
44. V. Kalchenko, Y. Kuznetsov, D. Preise, I. Meglinski, and A. Harmelin, "Ear Swelling Test by Using Laser Speckle Imaging with a Long Exposure Time," J. Biomed. Opt **19**(6), 060502 (2014).
45. S. L. Jacques, "Optical Properties of Biological Tissues: A Review," Phys. Med. Biol. **58**(11), R37–R61 (2013).
46. W. W. Focke, I. van der Westhuizen, N. Musee, and M. T. Loots, "Kinetic Interpretation of Log-Logistic Dose-Time Response Curves," Sci. Rep. **7**(1), 2234 (2017).
47. M. E. Brown and B. D. Glass, "Pharmaceutical Applications of the Prout–Tompkins Rate Equation," Int. J. Pharm. (Amsterdam, Neth.) **190**(2), 129–137 (1999).
48. A. Plonka, J. Mayer, D. Metodiewa, J. L. Gebicki, A. Zgirski, and M. Grabska, "Superoxide Radical Dismutation by Copper Proteins," J. Radioanal. Nucl. Chem. **101**(2), 221–225 (1986).
49. C. E. A. Souza, D. Maitra, G. M. Saed, M. P. Diamond, A. A. Moura, S. Pennathur, and H. M. Abu-Soud, "Hypochlorous Acid-Induced Heme Degradation from Lactoperoxidase as a Novel Mechanism of Free Iron Release and Tissue Injury in Inflammatory Diseases," PLoS One **6**(11), e27641 (2011).
50. C. M. Spickett, A. Jerlich, O. M. Panasenko, J. Arnhold, A. R. Pitt, T. Stelmaszyńska, and R. J. Schaur, "The Reactions of Hypochlorous Acid, the Reactive Oxygen Species Produced by Myeloperoxidase, with Lipids," Acta Biochim. Pol. (Engl. Transl.) **47**(4), 889–899 (2000).
51. S. Yamamoto, S. Shimizu, S. Kiyonaka, N. Takahashi, T. Wajima, Y. Hara, T. Negoro, T. Hiroi, Y. Kiuchi, T. Okada, S. Kaneko, I. Lange, A. Fleig, R. Penner, M. Nishi, H. Takeshima, and Y. Mori, "TRPM2-Mediated Ca2+ Influx Induces Chemokine Production in Monocytes That Aggravates Inflammatory Neutrophil Infiltration," Nat. Med. (N. Y., NY, U. S.) **14**(7), 738–747 (2008).
52. O. Soehnlein and L. Lindbom, "Phagocyte Partnership during the Onset and Resolution of Inflammation," Nat. Rev. Immunol. **10**(6), 427–439 (2010).
53. C. Nathan, "Neutrophils and Immunity: Challenges and Opportunities," Nat. Rev. Immunol. **6**(3), 173–182 (2006).
54. Y. Yang, A. V. Bazhin, J. Werner, and S. Karakhanova, "Reactive Oxygen Species in the Immune System," Int. Rev. Immunol. **32**(3), 249–270 (2013).
55. O. Soehnlein, L. Lindbom, and C. Weber, "Mechanisms Underlying Neutrophil-Mediated Monocyte Recruitment," Blood **114**(21), 4613–4623 (2009).
56. P. Holzer, "Neurogenic Vasodilatation and Plasma Leakage in the Skin," Gen. Pharmacol. **30**(1), 5–11 (1998).
57. O. A. Hatoum, H. Miura, and D. G. Binion, "The Vascular Contribution in the Pathogenesis of Inflammatory Bowel Disease," Am J Physiol Heart Circ Physiol **285**(5), H1791–H1796 (2003).
58. Z. Szekanecz and A. E. Koch, "Mechanisms of Disease: Angiogenesis in Inflammatory Diseases," Nat. Clin. Pract. Rheumatol. **3**(11), 635–643 (2007).
59. C. Liebetrau, J. Hoffmann, O. Dörr, L. Gaede, J. Blumenstein, H. Biermann, L. Pyttel, P. Thiele, C. Troidl, A. Berkowitsch, A. Rolf, S. Voss, C. W. Hamm, H. Nef, and H. Möllmann, "Release Kinetics of Inflammatory Biomarkers in a Clinical Model of Acute Myocardial Infarction," Circ. Res. **116**(5), 867–875 (2015).
60. B. A. Imhof, S. Jemelin, and Y. Emre, "Toll-like Receptors Elicit Different Recruitment Kinetics of Monocytes and Neutrophils in Mouse Acute Inflammation," Eur. J. Immunol. **47**(6), 1002–1008 (2017).
61. O. Holz, L. Tan, F. Schaumann, M. Müller, D. Scholl, R. Hidi, A. McLeod, N. Krug, and J. M. Hohlfeld, "Inter- and Intrasubject Variability of the Inflammatory Response to Segmental Endotoxin Challenge in Healthy Volunteers," Pulm. Pharmacol. Ther. **35**, 50–59 (2015).